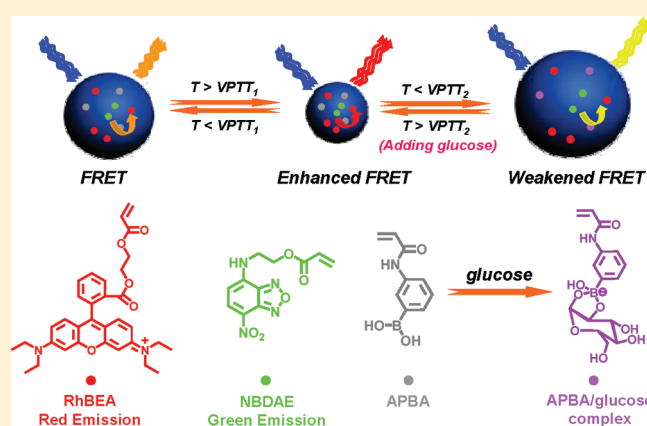


# Stimuli-Responsive Fluorescent Poly(*N*-isopropylacrylamide) Microgels Labeled with Phenylboronic Acid Moieties as Multifunctional Ratiometric Probes for Glucose and Temperatures

Di Wang, Tao Liu, Jun Yin, and Shiyong Liu\*

CAS Key Laboratory of Soft Matter Chemistry, Department of Polymer Science and Engineering, Hefei National Laboratory for Physical Sciences at the Microscale, University of Science and Technology of China, Hefei, Anhui 230026, China

**ABSTRACT:** We report on the fabrication of multifunctional ratiometric probes for glucose and temperatures based on thermo-responsive poly(*N*-isopropylacrylamide) (PNIPAM) microgels covalently incorporated with glucose-recognizing moieties, *N*-acryloyl-3-aminophenylboronic acid (APBA), fluorescence resonance energy transfer (FRET) donor dyes, 4-(2-acryloyloxyethylamino)-7-nitro-2,1,3-benzoxadiazole (NBDAE), and rhodamine B-based FRET acceptors (RhBEA). P(NIPAM-APBA-NBDAE-RhBEA) microgels containing FRET pairs and APBA were synthesized via free radical emulsion copolymerization. The spatial proximity of FRET donors and acceptors within microgels can be tuned via thermo-induced microgel collapse or glucose-induced microgel swelling at appropriate pH and temperatures, leading to the facile modulation of FRET efficiencies. APBA moieties within P(NIPAM-APBA-NBDAE-RhBEA) microgels can bind with glucose at appropriate pH to form cyclic boronate moieties, which can decrease the  $pK_a$  of APBA residues and increase the volume phase transition (VPT) temperature of microgels. The gradual addition of glucose into fluorescent microgel dispersions at intermediate temperatures, i.e., between microgel VPT temperatures in the absence and presence of glucose, respectively, can lead to the reswelling of initially collapsed microgels. Thus, P(NIPAM-APBA-NBDAE-RhBEA) microgels can serve as dual ratiometric fluorescent probes for glucose and temperatures by monitoring the changes in fluorescence emission intensity ratios. Moreover, P(NIPAM-APBA-NBDAE-RhBEA) microgels at pH 8 and 37 °C can serve as a ratiometric fluorescent glucose sensor with improved detection sensitivity as compared to that at 25 °C. MTT assays further revealed that thermo-responsive microgels are almost noncytotoxic up to a concentration of 1.6 g/L. These results augur well for the application of P(NIPAM-APBA-NBDAE-RhBEA) microgels for multifunctional purposes such as sensing, imaging, and triggered-release nanocarriers under in vivo conditions.



## INTRODUCTION

In the past decades, there has been a growing interest in stimuli-responsive microgels or nanogels due to their broad applications in diverse fields including nanoreactors, actuators, catalysis, drug delivery vehicles, and detection systems.<sup>1–13</sup> Stimuli-responsive microgels can undergo significant changes in size, hydrophilicity/hydrophobicity, and structural integrity under appropriate external stimuli such as pH, temperature, ionic strengths, light, electric/magnetic fields, biomolecules, and specific molecular recognition events.<sup>14–26</sup> This unique property of “intelligent” responses to external stimuli can be utilized to design sensing systems.<sup>27</sup> On the other hand, glucose is a particularly interesting target molecule owing to its inherent biological activities and physicochemical properties in living organisms. In this context, glucose-responsive microgels can play important roles in biomedicines and diabetes therapies. For example, microgels which can sense changes in blood glucose levels and intelligently regulate the release of insulin have been fabricated.<sup>28–40</sup>

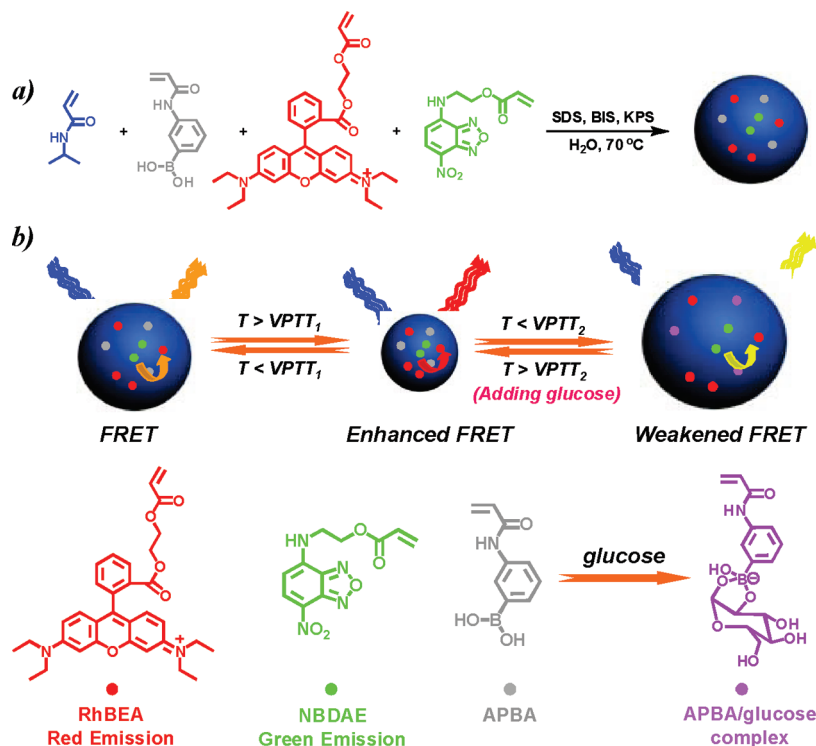
Previously, glucose-responsive hydrogels and microgels were prepared via the covalent or physical embedment of enzymes (e.g., glucose oxidase) or lectins (i.e., concanavalin A), which can either catalyze reactions or induce molecular recognition events with glucose.<sup>41–49</sup> Besides, phenylboronic acid moieties have also been frequently utilized to design glucose-responsive materials due to their unique reversible covalent interactions with *cis*-diol moiety in glucose to form cyclic boronate moieties.<sup>50–66</sup> Recently, Sumerlin et al.<sup>67</sup> successfully conducted reversible addition–fragmentation chain transfer (RAFT) polymerization of a protected phenylboronic acid (PBA) monomer, 4-pinacolatoborylstyrene (pBSt), and synthesized PBA-containing block copolymers. Later on, they further demonstrated a facile approach to the controlled synthesis of poly(*N*-acryloyl-3-aminophenylboronic acid)-*b*-poly(*N,N*-dimethylacrylamide), PAPBA-*b*-PDMA, via the RAFT polymerization of unprotected

Received: January 11, 2011

Revised: February 20, 2011

Published: March 11, 2011

**Scheme 1.** (a) Synthetic Schemes Employed for the Preparation of Thermo- and Glucose-Responsive P(NIPAM-APBA-NBDAE-RhBEA) Fluorescent Microgels via Emulsion Polymerization; (b) Schematic Illustration for the Modulation of FRET Efficiencies within P(NIPAM-APBA-NBDAE-RhBEA) Microgels by Temperature Variations and the Addition of Glucose



PBA monomers, and the obtained double hydrophilic block copolymer is dually responsive to glucose and pH.<sup>68</sup> Poly(*N*-isopropylacrylamide)-*b*-poly(*N*-acryloyl-3-aminophenylboronic acid), PNIPAM-*b*-PAPBA, which is triply responsive to temperature, pH, and glucose, was also reported by the same research group.<sup>69</sup> Shi et al.<sup>70,71</sup> fabricated micellar nanoparticles from 3-aminophenylboronic acid-modified poly(ethylene glycol)-*b*-poly(acrylic acid) (PEG-*b*-PAA) diblock copolymer and insulin, which exhibits glucose-regulated insulin release characteristics.

Poly(*N*-isopropylacrylamide) (PNIPAM) has been well-known for its lower critical solution temperature (LCST) phase behavior at  $\sim 32$  °C in aqueous solution. Accordingly, aqueous dispersions of PNIPAM microgels also exhibit similar volume phase transition (VPT) above a critical temperature (VPT temperature). Early in 1994, Kataoka et al.<sup>72</sup> reported the first synthesis of thermoresponsive polymers containing APBA residues, the LCST of which can be tuned via glucose addition. Recently, Ji et al.<sup>73</sup> synthesized double hydrophilic block copolymers containing a phenylboronic acid-functionalized thermoresponsive block, which exhibit multiple micellization behavior in response to pH, temperature, and glucose addition. They found that the LCST of the thermoresponsive block can shift from 21.2 to 25.5 °C upon addition of 50 mM glucose. Kataoka et al.<sup>74,75</sup> prepared PBA-based glucose-responsive hydrogels operating under physiological conditions, which offers an attractive option for the development of novel insulin delivery devices to treat diabetes. Cui and co-workers<sup>76</sup> reported the synthesis of triple-responsive (pH, thermo, and glucose) hydrogels from (2-dimethylamino)ethyl methacrylate (DMAEMA) and APBA and investigated the controlled release of bovine serum albumin (BSA) from these hydrogels. Ravaine's group<sup>31–33</sup> synthesized a

variety of glucose-responsive APBA-containing materials (such as microgels, core-shell microgels, and silica hybrid microgels) and investigated glucose-triggered insulin release properties. APBA-functionalized PNIPAM microgels or core-shell nanostructured microgels exhibiting thermo-induced VPT behavior were also reported by Zhang<sup>34–37</sup> and Hoare<sup>38,39</sup> research groups. They found that VPT temperatures can be tuned by glucose concentrations. They further reported that these novel types of responsive microgels can be utilized as the delivery and controlled-release nanocarriers of small molecules (e.g., Alizarin Red S) or proteins (e.g., insulin).

It is worthy of noting that in the above examples concerning glucose-responsive APBA-based microgels glucose only leads to changes in microgel sizes and collapse/swelling transitions, which is associated with the regulated release of insulin or other guest molecules. Under certain circumstances, it is highly desirable to more quantitatively monitor the changes of glucose concentrations and the correlation between insulin release kinetics and glucose concentrations under in vivo or in vitro conditions. Besides, imaging and sensing of glucose concentrations within living cells and tissues is also highly relevant to therapeutic protocols associated with diabetes. Ideally, multifunctional microgel nanocarriers capable of quantitatively sensing and fluorometric imaging of glucose concentrations and other physiologically relevant parameters (e.g., temperature and pH) and controlled or regulated release of bioactive molecules should provide indispensable advantages. In this context, the fluorometric technique is simple to perform and cost-effective and can offer high sensitivity for a variety of analytes.<sup>23–26,77–80</sup>

Previously, Zenkl et al.<sup>64,65</sup> prepared sugar-responsive fluorescent PNIPAM nanospheres containing APBA moieties and two

fluorophores (fluorescein and sulforhodamine B as FRET donor and acceptor, respectively) via precipitation polymerization. They focused on the monitoring of swelling kinetics in the presence of varying concentrations of sugar molecules at a fixed temperature (27 °C). The choice of these FRET pair dyes resulted in two poorly resolved emission peaks, and a direct correlation between the thermal phase transition temperatures and sugar concentrations has not been investigated. We recently reported an example of  $K^+$ - and thermo-sensing microgels consisting of NIPAM, FRET donor, and acceptor dyes and  $K^+$ -binding crown ether ligands. They can serve as ratiometric fluorescent  $K^+$  and temperature probes by monitoring the changes in fluorescence intensity ratios.<sup>26</sup>

Herein, we report on the fabrication of ratiometric fluorescent glucose sensors based on thermoresponsive PNIPAM microgels covalently incorporated with glucose-recognizing residues (APBA), FRET donor, 4-(2-acryloyloxyethylamino)-7-nitro-2,1,3-benzoxadiazole (NBDAE), and rhodamine B-based FRET acceptor (RhBEA) via the free radical emulsion copolymerization technique (see Scheme 1). We found that the detection performance of glucose is highly dependent on the temperature. Below the VPT temperature of glucose-free microgels at pH 8, the addition of glucose can drive the further expansion of initially swollen microgels due to the generation of negative charges within microgels, resulting from the  $pK_a$  shift of APBA residues from 8.7 to  $\sim 7$  upon glucose addition.<sup>72</sup> This process is accompanied by the decrease of fluorescence intensity ratios between acceptor and donor emissions. At temperatures between the VPT temperatures of microgels in the absence and presence of glucose, the addition of glucose leads to prominent microgel collapse–swelling transitions, accompanied by the dramatic decrease of fluorescence intensity ratios. Thus, higher glucose detection efficiencies can be achieved at elevated temperatures. Because of the thermoresponsiveness and the presence of ionizable APBA moieties within microgels, they can also serve as ratiometric fluorescent pH and temperature probes. Furthermore, MTT assays revealed that this novel type of thermoresponsive microgels is almost noncytotoxic up to a concentration of 1.6 g/L. All these results well support their applications for multifunctional purposes such as sensing, imaging, and triggered-release nanocarriers under *in vivo* conditions.

## EXPERIMENTAL SECTION

**Materials.** *N*-Isopropylacrylamide (97%, Tokyo Kasei Kagyo Co.) was recrystallized twice from benzene/hexane (1:3 v/v) prior to use. 3-Aminophenylboronic acid monohydrate (PBA, 98%) was purchased from Aldrich and used as received without further purification. *N,N'*-Methylenebis(acrylamide) (BIS) and ammonium persulfate (APS) were recrystallized from ethanol and methanol, respectively, and then stored at  $-20$  °C prior to use. Sodium dodecyl sulfate (SDS, 99%) was purchased from Alfa and used as received. *D*-Glucose (99%) was purchased from Acros. *N*-Acryloyl-3-aminophenylboronic acid (APBA),<sup>81</sup> 4-(2-acryloyloxyethylamino)-7-nitro-2,1,3-benzoxadiazole (NBDAE),<sup>82</sup> and rhodamine B-based FRET acceptor dye (RhBEA)<sup>79</sup> were prepared according to literature procedures (Scheme 1b). Water was deionized with a Milli-Q SP reagent water system (Millipore) to a specific resistivity of 18.4  $M\Omega \cdot cm$ .

Scheme 1a shows synthetic schemes employed for the preparation of thermo-, pH-, and glucose-responsive fluorescent P(NIPAM-APBA-NBDAE-RhBEA) microgels. Strategies employed for glucose-induced tuning of microgel VPT temperatures and thermo- and glucose-

modulated FRET efficiencies within responsive P(NIPAM-APBA-NBDAE-RhBEA) microgels are shown in Scheme 1b.

**Sample Preparation.** *Synthesis of P(NIPAM-APBA-NBDAE-RhBEA) Microgels.* Typical procedures employed for the synthesis of P(NIPAM-APBA-NBDAE-RhBEA) microgels with a APBA feed content of 10.0 mol % (relative to the sum of NIPAM and APBA) are as follows. NIPAM (0.34 g, 3 mmol), BIS (4 mg, 25  $\mu mol$ ), APBA (0.063 g, 0.33 mmol), SDS (17 mg, 0.06 mmol), and deionized water (40 mL) were charged into a 100 mL three-necked round-bottom flask equipped with a mechanical Teflon stirrer, reflux condenser, and a nitrogen gas inlet. After degassing by bubbling with nitrogen for 30 min and heating to 70 °C, KPS (21 mg, 0.08 mmol) dissolved in 1.0 mL of deionized water was injected under mechanical stirring at 400 rpm. NBDAE monomer (4.6 mg, 16.65  $\mu mol$ ) and RhBEA monomer (18 mg, 33.3  $\mu mol$ ) in 1.0 mL of ethanol were then added dropwise over  $\sim 20$  min. The polymerization was conducted under stirring at 70 °C for 7 h. Finally, the dispersion was passed through glass wool in order to remove particulates and then dialyzed against deionized water for 5 days. Fresh deionized water was replaced approximately every 6 h.

**In Vitro Cytotoxicity Measurement.** Cell viability was examined by the MTT assay. HeLa cells were seeded in a 96-well plate at an initial density of 5000 cells/well in 100  $\mu L$  of DMEM (Dulbecco's modified Eagle's medium) complete medium. Microgel dispersions were then added to achieve varying final concentrations. After incubation for 24 h, MTT reagent (in 20  $\mu L$  of PBS buffer, 5 mg/mL) was added to each well, and the cells were further incubated with 5%  $CO_2$  for 4 h at 37 °C. The culture medium in each well was removed and replaced by 100  $\mu L$  of DMSO. The solution from each well was transferred to another 96-well plate, and the absorbance values were recorded at a wavelength of 490 nm using a Thermo Electron MK3  $\mu m$ . The cell viability is calculated as  $A_{490,treated}/A_{490,control} \times 100\%$ , where  $A_{490,treated}$  and  $A_{490,control}$  are the absorbance values with or without the addition of microgels, respectively. Each experiment was done in quadruple. The data were shown as the mean value plus a standard deviation ( $\pm SD$ ).

**Characterization.** The optical transmittance of the microgel dispersion at a wavelength of 700 nm was acquired on a UV/vis TU-1901 spectrophotometer. A thermostatically controlled cuvette was employed, and the heating rate was 0.2 °C  $min^{-1}$ . The VPT temperature was defined as the temperature corresponding to  $\sim 1\%$  decrease in optical transmittance. For all temperature-dependent turbidimetry experiments, microgel concentrations were fixed at  $3.0 \times 10^{-4}$  g/mL. Field-emission scanning electron microscope (FE-SEM) observations were conducted on a high-resolution JEOL JSM-6700 field-emission scanning electron microscopy. The samples for SEM observations were prepared by placing 10  $\mu L$  of microgel solutions on copper grids successively coated with thin films of Formvar and carbon. Atomic force microscope (AFM) measurements were performed on a Digital Instrument Multimode Nanoscope IIID operating in the tapping mode under ambient conditions. A silicon cantilever (RFESP) with resonance frequency of  $\sim 80$  kHz and spring constant of  $\sim 3$  N/m was used. The set-point amplitude ratio was maintained at 0.7 to minimize sample deformation induced by the tip. The sample was prepared by dip-coating the microgel dispersion onto freshly cleaved mica surface, followed by natural drying. Dynamic and static laser light scattering (LLS) measurements were conducted on a commercial spectrometer (ALV/DLS/SLS-5022F) equipped with a multitau digital time correlator (ALV5000) and a cylindrical 22 mW UNIPHASE He–Ne laser ( $\lambda_0 = 632$  nm) as the light source. Scattered light was collected at a fixed angle of 90° for a duration of  $\sim 5$  min. Distribution averages and particle size distributions were computed using cumulants analysis and CONTIN routines. All data were averaged over three measurements, and the microgel concentrations were fixed at  $1.0 \times 10^{-4}$  g/mL. Fluorescence spectra were recorded using a F-4600 (Hitachi) spectrofluorometer. The temperature

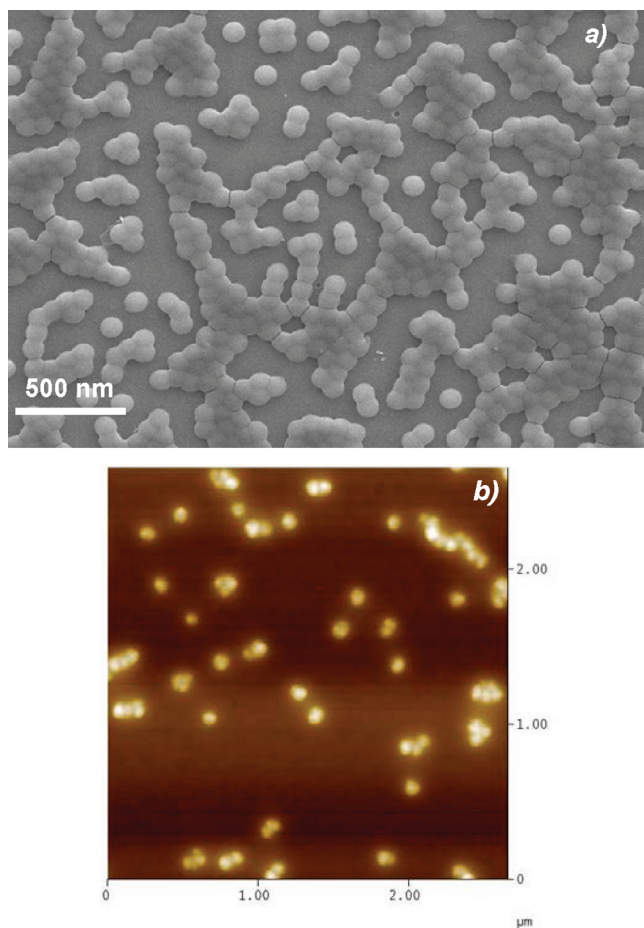


**Figure 1.** (a) SEM and (b) AFM height images obtained for P(NIPAM-APBA-NBDAE-RhBEA) microgels.

of the water-jacketed cell holder was controlled by a programmable circulation bath. The slit widths were set at 5 nm for excitation and 5 nm for emission. For all microgel-based fluorescence measurements, microgel concentrations were fixed at  $1.0 \times 10^{-4}$  g/mL. Inverted fluorescence microscope was performed on an Olympus IX71 microscope equipped with a temperature-regulated incubator (450–480 nm exciter filter and long pass 515 nm barrier filter).

## RESULTS AND DISCUSSION

Synthetic schemes employed for the preparation of thermo- and glucose-responsive P(NIPAM-APBA-NBDAE-RhBEA) fluorescent microgels and the schematic illustration for the modulation of FRET efficiencies within the microgels by temperature variations and the addition of glucose are shown in Scheme 1. At intermediate temperatures, i.e., between VPT temperatures of the microgels in the absence and presence of glucose, respectively, the FRET donors and acceptors within microgels are in close proximity due to that microgels are in the collapsed state, and this is associated with high FRET efficiency; upon addition of glucose, the microgels are subjected to swelling due to the elevation of VPT temperatures, accompanied by the considerable decrease of FRET efficiencies. Thus, thermoresponsive P(NIPAM-APBA-NBDAE-RhBEA) fluorescent microgels can exhibit multicolor emissions tunable by temperature variations and glucose concentrations.

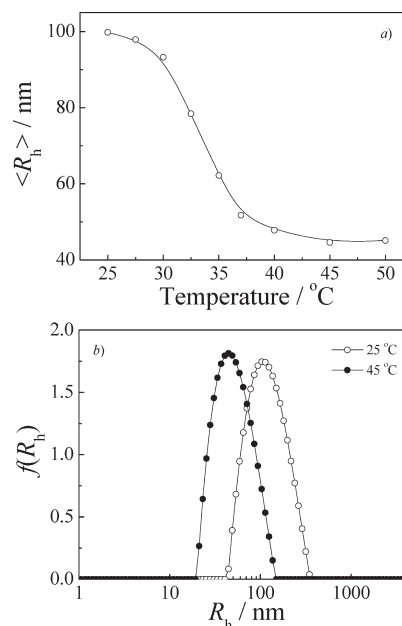


**Figure 2.** (a) Temperature-dependent intensity-average hydrodynamic radius,  $\langle R_h \rangle$ , and (b) typical hydrodynamic radius distributions,  $f(R_h)$ , at 25 °C (○) and 45 °C (●), respectively, recorded for 0.1 g/L aqueous dispersion of P(NIPAM-APBA-NBDAE-RhBEA) microgels (pH 8.0, prepared at a APBA feed ratio of 10 mol %) in the absence of glucose.

**Thermo-Regulated Volume Phase Transitions and FRET Efficiencies of P(NIPAM-APBA-NBDAE-RhBEA) Microgels.** As shown in Scheme 1a, P(NIPAM-APBA-NBDAE-RhBEA) microgels possessing a feed cross-linking density of 1.0 wt % (relative to the sum of NIPAM and APBA) and 10.0 mol % feed contents of APBA monomer (relative to the sum of NIPAM and APBA) were synthesized via free radical emulsion copolymerization of NIPAM, APBA, and polymerizable FRET donor and acceptor dyes (NBDAE and RhBEA) in the presence of BIS and SDS at around neutral pH and 70 °C. Figure 1 shows the SEM and AFM images recorded for the aqueous dispersion of P(NIPAM-APBA-NBDAE-RhBEA) microgels at 25 °C, revealing the presence of fairly monodisperse and spherical nanoparticles with an average diameter of ~95 nm.

Figure 2 shows temperature-dependent intensity-average hydrodynamic radius,  $\langle R_h \rangle$ , recorded for P(NIPAM-APBA-NBDAE-RhBEA) microgels (pH 8.0, 0.1 g/L) in the absence of glucose as determined by dynamic LLS. Upon heating,  $\langle R_h \rangle$  decreases from ~100 nm at 25 °C to 43 nm at 45 °C, i.e., ~12.6 times of decrease in microgel hydrodynamic volumes. From Figure 2a, we can tell that prominent microgel collapse occurs at temperatures above ~30 °C, which should be ascribed to the VPT of P(NIPAM-APBA-NBDAE-RhBEA) microgels. Figure 2b shows typical hydrodynamic radius distributions,  $f(R_h)$ , at 25 and 45 °C, respectively, with the polydispersity index,  $\mu_2/\Gamma^2$ , being 0.08 and 0.03, respectively. Since SEM and AFM determine nanoparticle dimensions in the dry state, whereas dynamic LLS reports intensity-average dimensions in solution, the dynamic LLS results are in reasonable agreement with those determined by SEM and AFM (see Figure 1).

It is well-known that the FRET process is associated with the energy transfer between two chromophores, the efficiency of which highly depends on the spatial distance between donor and acceptor moieties. Because of the sensitivity of fluorometric

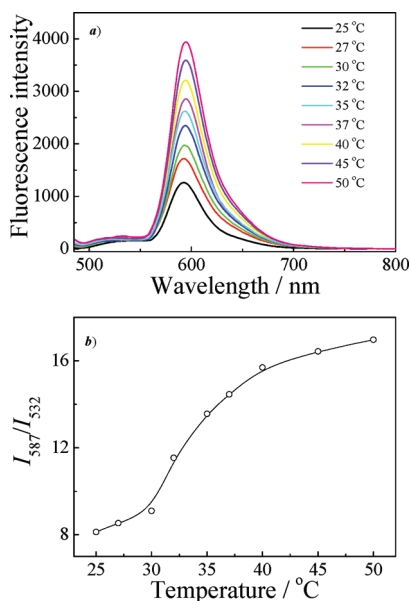


**Figure 3.** (a) Fluorescence emission spectra and (b) fluorescence intensity ratio changes ( $I_{587}/I_{532}$ ,  $\lambda_{\text{ex}} = 470$  nm; slit widths: Ex. 5 nm, Em. 5 nm) recorded for 0.1 g/L aqueous dispersion of P(NIPAM-APBA-NBDAE-RhBEA) microgels (pH 8.0, prepared at a APBA feed ratio of 10 mol %) in the absence of glucose at varying temperatures.

technique and the detection principle, changes in FRET efficiencies has been previously employed to probe detailed local information on the VPT process of thermoresponsive microgels.<sup>77,78</sup> In this context, Lyon and co-workers<sup>77,78</sup> previously reported excellent examples of tracing the VPT process of thermoresponsive microgels simultaneously labeled with FRET donor and acceptor dyes by monitoring changes in FRET efficiencies. Accordingly, the collapse or swelling of P(NIPAM-APBA-NBDAE-RhBEA) microgels covalently attached with FRET pairs can be quantified by changes in FRET efficiencies, in addition to microgel size changes. In the current study, NBDAE and RhBEA dyes are chosen as the FRET donor and acceptor, respectively, due to the excellent overlap between the emission spectrum of NBDAE and the excitation spectrum of RhBEA moieties.<sup>79</sup>

Figure 3 shows temperature-dependent fluorescence emission spectra and changes in fluorescence intensity ratios ( $I_{587}/I_{532}$ ,  $\lambda_{\text{ex}} = 470$  nm) recorded for 0.1 g/L aqueous dispersion of P(NIPAM-APBA-NBDAE-RhBEA) microgels (pH 8.0) in the absence of glucose. Two fluorescence emission peaks at around 532 and 587 nm can be apparently observed, which are ascribed to the fluorescence emission of NBDAE and RhBEA moieties, respectively. With the increase of temperature, the intensity of emission band at 587 nm increases prominently. It is quite surprising that the emission band of NBDAE at  $\sim 532$  nm almost does not exhibit any intensity changes. This can be ascribed to the two competing factors. With the increase of temperature, the collapse of microgels will lead to the increase of NBDAE emission due to the formation of more hydrophobic microenvironment.<sup>83</sup> On the other hand, the closer proximity between NBDAE/RhBEA FRET pair will lead to the decrease of NBD emission intensity due to more effective FRET processes. Moreover, at pH 8.0, some APBA residues, possessing a  $\text{p}K_{\text{a}}$  of  $\sim 8.7$ , exist in the deionized form, and preliminary experiments revealed that APBA in the deionized form can partially quench

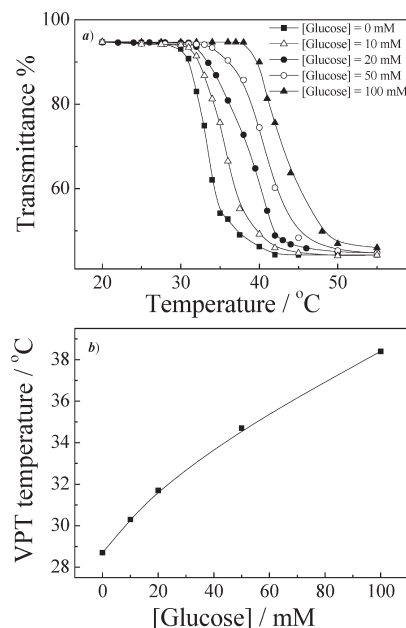


**Figure 4.** (a) Temperature-dependent optical transmittance at a wavelength of 700 nm recorded for 0.3 g/L aqueous dispersion of P(NIPAM-APBA-NBDAE-RhBEA) microgels (pH 8.0, prepared at a APBA feed ratio of 10 mol %) in the presence of varying glucose concentrations. (b) Variation of VPT temperatures of 0.3 g/L aqueous dispersion of P(NIPAM-APBA-NBDAE-RhBEA) microgels (pH 8.0) as a function of glucose concentrations. VPT temperatures were defined as the temperature corresponding to  $\sim 1\%$  decrease in optical transmittance. The measurements were conducted 4 h after addition of glucose.

the fluorescence emission of NBDAE. All the above factors lead to the observed almost constant emission intensity of NBDAE residues over the temperature range of 25–50 °C. From Figure 3b, we can see that the fluorescence intensity ratios,  $I_{587}/I_{532}$ , considerably increase from  $\sim 8$  at 25 °C to  $\sim 17$  at 45 °C. This clearly reflected that the microgel collapse at elevated temperatures can lead to prominent enhancement of FRET efficiencies within P(NIPAM-APBA-NBDAE-RhBEA) microgels.

**Glucose-Regulated Volume Phase Transitions of P(NIPAM-APBA-NBDAE-RhBEA) Microgels.** Similar to those exhibited by PNIPAM homopolymers, the copolymerization of hydrophilic or hydrophobic monomers into PNIPAM microgels can also increase or decrease the VPT temperatures, respectively. APBA residues possess a  $\text{p}K_{\text{a}}$  of  $\sim 8.7$ ; thus, the change of pH across the  $\text{p}K_{\text{a}}$  leads to the transformation between hydrophilic ionized state and relatively hydrophobic deionized state. On the other hand, the addition of glucose can also shift the  $\text{p}K_{\text{a}}$  to lower values ( $\sim 7$ ) via the formation of cyclic boronate moieties from APBA residues and glucose;<sup>72</sup> at a constant pH (e.g., pH 8), this will also lead to a shift in the hydrophilic/hydrophobic balance of the microgels.

Temperature-dependent optical transmittance measurements were employed to determine the changes of VPT temperature (defined as the temperature corresponding to  $\sim 1\%$  decrease in optical transmittance) of P(NIPAM-APBA-NBDAE-RhBEA) microgels upon addition of varying amounts of glucose at pH 8 (see Figure 4). In the absence of glucose, the VPT temperature of the microgel is around 28.7 °C, which is lower than conventional PNIPAM microgels, indicating that the copolymerization

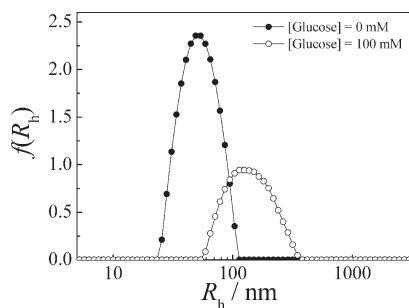


**Figure 5.** Typical hydrodynamic radius distributions,  $f(R_h)$ , recorded for 0.1 g/L aqueous dispersions of P(NIPAM-APBA-NBDAE-RhBEA) microgels (pH 8.0, prepared at a APBA feed ratio of 10 mol %) at 37 °C in the absence (●) and presence (○) of 100 mM glucose, respectively.

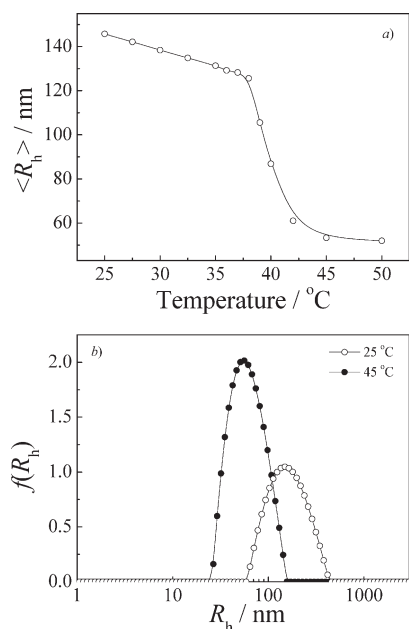


**Figure 6.** (a) Temperature-dependent intensity-average hydrodynamic radius,  $\langle R_h \rangle$ , and (b) typical hydrodynamic radius distributions,  $f(R_h)$ , at 25 °C (○) and 45 °C (●), respectively, recorded for 0.1 g/L aqueous dispersion of P(NIPAM-APBA-NBDAE-RhBEA) microgels (pH 8.0, prepared at a APBA feed ratio of 10 mol %) in the presence of 100 mM glucose.

of ~10 mol % APBA residues into the microgels (at pH 8) can render them less hydrophilic. This is understandable considering that at pH 8 certain APBA residues are in the deionized state. As the concentration of glucose increased to 100 mM, the VPT temperature of microgels increased to 38.4 °C (Figure 4b). The almost linear increase of VPT temperatures for APBA-containing PNIPAM microgels in the presence of increasing amounts of glucose has previously been reported by several research groups.<sup>36,38</sup> Hoare et al.<sup>38</sup> observed that as the glucose concentration increases from 0 to about 20 mM ~4 °C increase of VPT temperature can be determined for P(NIPAM-AA) microgels functionalized with 3-aminophenylboronic acid, where AA is acrylic acid. Zhang and co-workers<sup>36</sup> also synthesized APBA-functionalized PNIPAM microgels and observed similar effects of glucose concentration on the VPT temperatures.

Figure 5 gives typical hydrodynamic radius distributions,  $f(R_h)$ , recorded for 0.1 g/L aqueous dispersions of P(NIPAM-

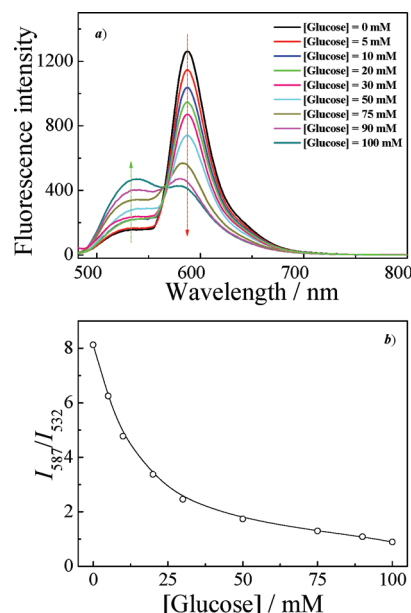


**Figure 7.** (a) Fluorescence emission spectra and (b) fluorescence intensity ratio changes ( $I_{587}/I_{532}$ ,  $\lambda_{\text{ex}} = 470$  nm; slit widths: Ex. 5 nm, Em. 5 nm) recorded for 0.1 g/L aqueous dispersion of P(NIPAM-APBA-NBDAE-RhBEA) microgels (prepared at a APBA feed ratio of 10 mol %) upon gradual addition of glucose at 25 °C and pH 8.0. Each spectrum was acquired 4 h after glucose addition.

APBA-NBDAE-RhBEA) microgels (pH 8.0) at 37 °C in the absence and presence of 100 mM glucose, respectively. The solution temperature was fixed at 37 °C, which is above the VPT temperature of microgels in the absence of glucose but below the VPT of microgels in the presence of 100 mM glucose. At 37 °C and pH 8.0, the as-synthesized microgels possess a  $\langle R_h \rangle$  of ~50 nm, which are in the collapsed state (Figure 2). Upon addition of 100 mM glucose, the  $\langle R_h \rangle$  increases to ~130 nm, clearly indicating that the addition of glucose can lead to the microgel collapse/swelling transition at intermediate temperatures. This can be ascribed to the fact that the addition glucose can render the microgels more hydrophilic due to the generation of negative charges and the considerable shift of microgel VPT temperature to above 37 °C (Figure 4).

In the presence of 100 mM glucose, P(NIPAM-APBA-NBDAE-RhBEA) microgels also exhibit thermo-induced collapse, but at considerably elevated temperatures. The temperature-dependent intensity-average hydrodynamic radius,  $\langle R_h \rangle$ , recorded for 0.1 g/L aqueous dispersion of microgels (pH 8.0) in the presence of 100 mM glucose is shown in Figure 6a, and we can discern an inflection point at ~38 °C. This result correlates well with the temperature-dependent optical transmittance results (see Figure 4). Figure 6b shows that P(NIPAM-APBA-NBDAE-RhBEA) microgels exhibit  $\langle R_h \rangle$  of ~145 and ~50 nm at 25 and 45 °C, respectively, which are systematically higher than those of microgels in the absence of glucose but at comparable temperatures.

The VPT of microgels induced by temperature variations (Figures 2 and 6) or by the addition of glucose at appropriate temperature ranges (Figure 5) can also be quantified by the changes in FRET efficiencies due to that the phase transition can also lead to considerable changes in the spatial distributions of FRET donors and acceptors within P(NIPAM-APBA-NBDAE-RhBEA) microgels. Figure 7 shows the fluorescence emission

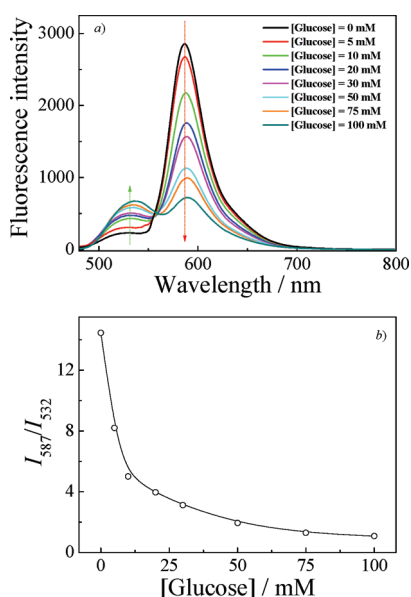


**Figure 8.** (a) Fluorescence emission spectra and (b) fluorescence intensity ratio changes ( $I_{587}/I_{532}$ ,  $\lambda_{\text{ex}} = 470$  nm; slit widths: Ex. 5 nm, Em. 5 nm) recorded for 0.1 g/L aqueous dispersion of P(NIPAM-APBA-NBDAE-RhBEA) microgels (prepared at a APBA feed ratio of 10 mol %) upon gradual addition of glucose at 37 °C and pH 8.0. Each spectrum was acquired 4 h after glucose addition.

spectra and fluorescence intensity ratio changes ( $I_{587}/I_{532}$ ,  $\lambda_{\text{ex}} = 470$  nm) recorded for 0.1 g/L aqueous dispersion of P(NIPAM-APBA-NBDAE-RhBEA) microgels at 25 °C and pH 8.0 upon addition of varying amounts of glucose. From Figure 7a, we can observe that, with the increase of glucose concentrations, the emission intensity at 532 nm increased considerably, accompanied by the intensity decrease of emission band at 587 nm. The observed prominent decrease of FRET efficiencies can be well correlated to the further swelling to  $\sim 145$  nm for microgels initially in the swollen state ( $\sim 100$  nm), which has already been verified by LLS results (Figures 2a and 6a). The fluorescence intensity ratios,  $I_{587}/I_{532}$ , decreased from  $\sim 8.0$  to 0.8 in the glucose range of 0–100 mM at 25 °C (see Figure 7b). This indicated that although P(NIPAM-APBA-NBDAE-RhBEA) microgels are in the swollen state at 25 °C, they can still serve as excellent ratiometric fluorometric glucose probes.

If the temperature was maintained between two critical values (i.e.,  $\text{VPTT}_1$  and  $\text{VPTT}_2$ , which represent microgel VPT temperatures in the absence and presence of glucose, respectively), microgels will be in the collapsed state initially and subjected to swelling transitions upon addition of glucose (Figure 5). From Figure 8a, we can see that at 37 °C the emission intensity ratios,  $I_{587}/I_{532}$ , decreased from  $\sim 14.5$  to 1 in the glucose concentration range of 0–100 mM. The more dramatic changes in emission intensity ratios compared to that at 25 °C should be ascribed to the more prominent volumetric changes of microgels (25 °C: 100–145 nm in the presence of 0–100 mM glucose; 37 °C: 50–130 nm in the presence of 0–100 mM glucose).

It has been well-known that the normal blood glucose concentration is in the range of 3.5–6.1 mM and abnormal glucose levels can reach as high as  $\sim 20$  mM.<sup>30,84</sup> A comparison between Figures 7b and 8b revealed that at 37 °C thermoresponsive P(NIPAM-APBA-NBDAE-RhBEA) microgels possess much better glucose detection sensitivity as compared to those

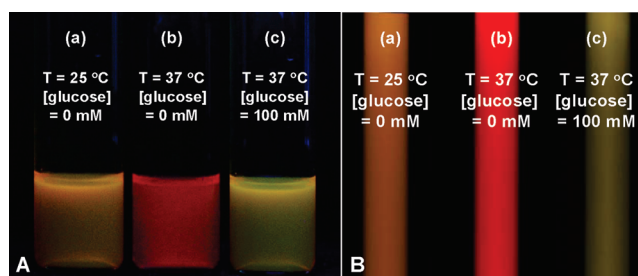


**Figure 9.** Photographs recorded (A) under 365 nm UV lamp and (B) inverted fluorescence microscopy equipped with a temperature-regulated incubator (450–480 nm exciter filter and long pass 515 nm barrier filter) for 0.3 g/L aqueous dispersion of P(NIPAM-APBA-NBDAE-RhBEA) microgels (pH 8.0, prepared at a APBA feed ratio of 10 mol %) under various conditions: (a) 25 °C, [glucose] = 0 mM; (b) 37 °C, [glucose] = 0 mM; (c) 37 °C, [glucose] = 100 mM.

at 25 °C. Emission intensity ratios,  $I_{587}/I_{532}$ , of P(NIPAM-APBA-NBDAE-RhBEA) microgels at 25 °C decreased  $\sim 4.8$ -fold (from 8.1 to 1.7) in the glucose concentration range of 0–50 mM, whereas for microgels at 37 °C, the intensity ratios exhibit  $\sim 7.6$ -fold decrease (from 14.5 to 1.9) in the same glucose concentration range. Thus, the current system further confirmed that the responsiveness of polymeric microgels can be utilized to design novel sensing systems with tunable detection sensitivities. Most importantly, the variation of temperatures in the absence of glucose and the addition of glucose at 37 °C can lead to clearly evident fluorometric transitions, which can be both checked by the naked eye or more accurately under an inverted fluorescence microscopy. From Figure 9, we can observe that an orange-to-red emission transition is associated with heating process from 25 to 37 °C, whereas the addition of 100 mM glucose leads to the fluorometric transition from red to yellowish at 37 °C. Thus, the above results have established that thermoresponsive P(NIPAM-APBA-NBDAE-RhBEA) microgels labeled with FRET pair can serve as dual ratiometric fluorometric probes for both temperatures and glucose.

**pH-Regulated Volume Phase Transitions of Microgels and In Vitro Cytotoxicity Measurements.** Since the ionization–deionization equilibrium of APBA moieties can also be shifted by pH variations in addition to glucose addition, we further examined the VPT phase transition of P(NIPAM-APBA-NBDAE-RhBEA) microgels at varying pH conditions. Temperature-dependent optical transmittance measurements (Figure 10a) at pH 11 indicated that the VPT temperature of microgel increased to  $\sim 37$  °C, which are much higher than the VPT temperature of 28.7 °C for microgels at pH 8.0 (Figure 4a). Figure 10b shows typical fluorescence emission spectra recorded for 0.1 g/L aqueous dispersion of P(NIPAM-APBA-NBDAE-RhBEA) microgels in the absence of glucose at pH 8.0 and 11.0, respectively (37 °C). The increase of solution pH from 8 to 11 again leads to the considerable decrease of FRET efficiencies due to the prominent swelling of microgels resulting from the generation of negative charges and the increase of VPT temperatures at elevated pH conditions. In combination with the results shown in previous sections, we successfully demonstrated that FRET processes occurred within thermoresponsive microgels covalently labeled with APBA moieties, and FRET pairs can be utilized to construct ratiometric fluorometric multifunctional probes for temperature, glucose, and pH. Compared to conventional characterization techniques relevant to size changes

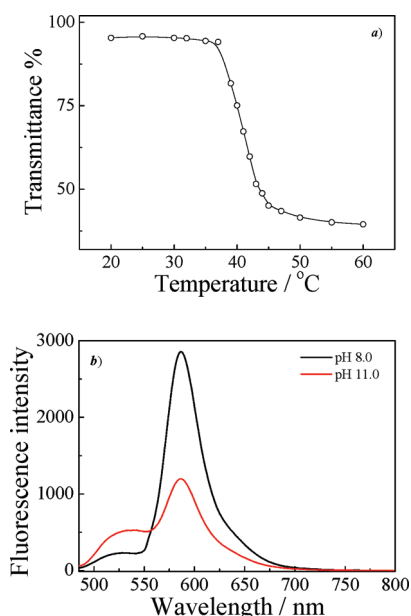


**Figure 10.** (a) Temperature-dependent optical transmittance at a wavelength of 700 nm recorded for 0.3 g/L aqueous dispersion of P(NIPAM-APBA-NBDAE-RhBEA) microgels (pH 11.0, prepared at a APBA feed ratio of 10 mol %) in the absence of glucose. (b) Typical fluorescence emission spectra ( $\lambda_{\text{ex}} = 470$  nm; slit widths: Ex. 5 nm, Em. 5 nm, 37 °C) recorded for 0.1 g/L aqueous dispersion of P(NIPAM-APBA-NBDAE-RhBEA) microgels (prepared at a APBA feed ratio of 10 mol %) at pH 8.0 and pH 11.0, respectively.

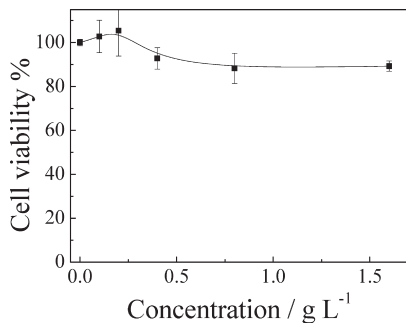


**Figure 11.** In vitro cytotoxicity of P(NIPAM-APBA-NBDAE-RhBEA) microgels against HeLa cells as a function of microgel concentrations determined by the MTT assay.

induced by microgel VPTs, the introduction of FRET principle into APBA-containing PNIPAM microgels allows for the construction of a convenient, cost-effective, quantitative, and multifunctional sensing system. Finally, we have further examined the in vitro cell cytotoxicity of P(NIPAM-APBA-NBDAE-RhBEA) microgels by the MTT assay, and the results are shown in Figure 11. HeLa cells were treated with microgel dispersions at varying concentrations. The cell viability remained to be  $\sim 90\%$  even at a microgel concentration of 1.6 mg/mL, indicating that the reported thermoresponsive P(NIPAM-APBA-NBDAE-RhBEA) microgels are almost noncytotoxic.

## CONCLUSIONS

In summary, we synthesized fluorescent thermoresponsive PNIPAM microgels covalently incorporated with glucose-

recognizing residues, APBA, FRET donor dyes, 4-(2-acryloyloxyethylamino)-7-nitro-2,1,3-benzoxadiazole (NBDAE), and rhodamine B-based FRET acceptors (RhBEA) via the free radical emulsion copolymerization technique. The as-synthesized P(NIPAM-APBA-NBDAE-RhBEA) microgels can serve as multifunctional ratiometric fluorometric probes for glucose and temperatures. The spatial proximity between FRET donors and acceptors within microgels can be tuned via thermo-induced microgel collapse or glucose-induced microgel swelling at appropriate pH and temperatures. FRET efficiencies between NBDAE and RhBEA moieties were then employed to monitor the thermo-induced microgel collapse and glucose-induced microgel swelling. The latter is due to the generation of negative charges resulting from the binding of glucose with APBA to form cyclic boronate moieties and the  $pK_a$  decrease of APBA residues. At pH 8, P(NIPAM-APBA-NBDAE-RhBEA) microgels at 37 °C can serve as a ratiometric fluorescent glucose sensor with much more improved detection sensitivity as compared to that at 25 °C. MTT assays further revealed that the reported thermoresponsive microgels are almost noncytotoxic up to a concentration of 1.6 g/L. We expect that the reported microgel system can serve as smart nanocarriers for multifunctional purposes including sensing, imaging, and triggered release under in vivo conditions, and further investigations toward this aspect are currently under way in our laboratory.

## AUTHOR INFORMATION

### Corresponding Author

\*E-mail: sliu@ustc.edu.cn.

## ACKNOWLEDGMENT

The financial support from National Natural Scientific Foundation of China (NNSFC) Project (20874092, 91027026, and 51033005) and Fundamental Research Funds for the Central Universities is gratefully acknowledged.

## REFERENCES

- (1) Bailey, R. C.; Nam, J. M.; Mirkin, C. A.; Hupp, J. T. *J. Am. Chem. Soc.* **2003**, *125*, 13541–13547.
- (2) Kim, J.; Nayak, S.; Lyon, L. A. *J. Am. Chem. Soc.* **2005**, *127*, 9588–9592.
- (3) Kumar, A.; Srivastava, A.; Galaev, I. Y.; Mattiasson, B. *Prog. Polym. Sci.* **2007**, *32*, 1205–1237.
- (4) Malmsten, M.; Bysell, H.; Hansson, P. *Curr. Opin. Colloid Interface Sci.* **2010**, *15*, 435–444.
- (5) Motornov, M.; Roiter, Y.; Tokarev, I.; Minko, S. *Prog. Polym. Sci.* **2010**, *35*, 174–211.
- (6) Nayak, S.; Lyon, L. A. *Angew. Chem., Int. Ed.* **2004**, *43*, 6706–6709.
- (7) Nolan, C. M.; Reyes, C. D.; Debord, J. D.; Garcia, A. J.; Lyon, L. A. *Biomacromolecules* **2005**, *6*, 2032–2039.
- (8) Roy, D.; Cambre, J. N.; Sumerlin, B. S. *Prog. Polym. Sci.* **2010**, *35*, 278–301.
- (9) Serpe, M. J.; Kim, J.; Lyon, L. A. *Adv. Mater.* **2004**, *16*, 184–187.
- (10) Soppimath, K. S.; Tan, D. C. W.; Yang, Y. Y. *Adv. Mater.* **2005**, *17*, 318–323.
- (11) Tokarev, I.; Minko, S. *Adv. Mater.* **2010**, *22*, 3446–3462.
- (12) Zhang, H.; Mardiyani, S.; Chan, W. C. W.; Kumacheva, E. *Biomacromolecules* **2006**, *7*, 1568–1572.
- (13) Qiu, Y.; Park, K. *Adv. Drug Delivery Rev.* **2001**, *53*, 321–339.
- (14) Debord, J. D.; Lyon, L. A. *Langmuir* **2003**, *19*, 7662–7664.

- (15) Amalvy, J. I.; Wanless, E. J.; Li, Y.; Michailidou, V.; Armes, S. P.; Duccini, Y. *Langmuir* **2004**, *20*, 8992–8999.
- (16) Das, M.; Mardiyani, S.; Chan, W. C. W.; Kumacheva, E. *Adv. Mater.* **2006**, *18*, 80–83.
- (17) Garcia, A.; Marquez, M.; Cai, T.; Rosario, R.; Hu, Z. B.; Gust, D.; Hayes, M.; Vail, S. A.; Park, C. D. *Langmuir* **2007**, *23*, 224–229.
- (18) Fujii, S.; Dupin, D.; Araki, T.; Armes, S. P.; Ade, H. *Langmuir* **2009**, *25*, 2588–2592.
- (19) Perez-Alvarez, L.; Saez-Martinez, V.; Hernaez, E.; Katime, I. *Macromol. Chem. Phys.* **2009**, *210*, 1120–1126.
- (20) Hoare, T.; Pelton, R. *Macromolecules* **2004**, *37*, 2544–2550.
- (21) Yin, J.; Dupin, D.; Li, J. F.; Armes, S. P.; Liu, S. Y. *Langmuir* **2008**, *24*, 9334–9340.
- (22) Bromberg, L.; Temchenko, M.; Hatton, T. A. *Langmuir* **2002**, *18*, 4944–4952.
- (23) Liu, T.; Hu, J. M.; Yin, J.; Zhang, Y. F.; Li, C. H.; Liu, S. Y. *Chem. Mater.* **2009**, *21*, 3439–3446.
- (24) Li, C. H.; Liu, S. Y. *J. Mater. Chem.* **2010**, *20*, 10716–10723.
- (25) Yin, J.; Hu, H. B.; Wu, Y. H.; Liu, S. Y. *Polym. Chem.* **2011**, *2*, 363–371.
- (26) Yin, J.; Li, C. H.; Wang, D.; Liu, S. Y. *J. Phys. Chem. B* **2010**, *114*, 12213–12220.
- (27) Hu, J. M.; Liu, S. Y. *Macromolecules* **2010**, *43*, 8315–8330.
- (28) Wu, W. T.; Mitra, N.; Yan, E. C. Y.; Zhou, S. Q. *ACS Nano* **2010**, *4*, 4831–4839.
- (29) Wu, W. T.; Zhou, T.; Shen, J.; Zhou, S. Q. *Chem. Commun.* **2009**, 4390–4392.
- (30) Shiino, D.; Kataoka, K.; Koyama, Y.; Yokoyama, M.; Okano, T.; Sakurai, Y. *J. Intell. Mater. Syst. Struct.* **1994**, *5*, 311–314.
- (31) Lapeyre, V.; Ancla, C.; Catargi, B.; Ravaine, V. *J. Colloid Interface Sci.* **2008**, *327*, 316–323.
- (32) Lapeyre, V.; Gosse, I.; Chevreux, S.; Ravaine, V. *Biomacromolecules* **2006**, *7*, 3356–3363.
- (33) Lapeyre, V.; Renaudie, N.; Dechezelles, J. F.; Saadaoui, H.; Ravaine, S.; Ravaine, V. *Langmuir* **2009**, *25*, 4659–4667.
- (34) Zhang, Y. J.; Guan, Y.; Zhou, S. Q. *Biomacromolecules* **2007**, *8*, 3842–3847.
- (35) Liu, P. X.; Luo, Q. F.; Guan, Y.; Zhang, Y. J. *Polymer* **2010**, *51*, 2668–2675.
- (36) Zhang, Y. J.; Guan, Y.; Zhou, S. Q. *Biomacromolecules* **2006**, *7*, 3196–3201.
- (37) Luo, Q. F.; Liu, P. X.; Guan, Y.; Zhang, Y. J. *ACS Appl. Mater. Interfaces* **2010**, *2*, 760–767.
- (38) Hoare, T.; Pelton, R. *Macromolecules* **2007**, *40*, 670–678.
- (39) Hoare, T.; Pelton, R. *Biomacromolecules* **2008**, *9*, 733–740.
- (40) Shiino, D.; Murata, Y.; Kataoka, K.; Koyama, Y.; Yokoyama, M.; Okano, T.; Sakurai, Y. *Biomaterials* **1994**, *15*, 121–128.
- (41) Hassan, C. M.; Doyle, F. J.; Peppas, N. A. *Macromolecules* **1997**, *30*, 6166–6173.
- (42) Miyata, T.; Uragami, T.; Nakamae, K. *Adv. Drug Delivery Rev.* **2002**, *54*, 79–98.
- (43) Sierra, J. F.; Galban, J.; Castillo, J. R. *Anal. Chem.* **1997**, *69*, 1471–1476.
- (44) Sanz, V.; Galban, J.; de Marcos, S.; Castillo, J. R. *Talanta* **2003**, *60*, 415–423.
- (45) Russell, R. J.; Pishko, M. V.; Geffrides, C. C.; McShane, M. J.; Cote, G. L. *Anal. Chem.* **1999**, *71*, 3126–3132.
- (46) Miyata, T.; Jikihara, A.; Nakamae, K.; Hoffman, A. S. *Macromol. Chem. Phys.* **1996**, *197*, 1135–1146.
- (47) Traitel, T.; Cohen, Y.; Kost, J. *Biomaterials* **2000**, *21*, 1679–1687.
- (48) Lim, C. K.; Lee, Y. D.; Na, J.; Oh, J. M.; Her, S.; Kim, K.; Choi, K.; Kim, S.; Kwon, I. C. *Adv. Funct. Mater.* **2010**, *20*, 2644–2648.
- (49) Miyata, T.; Jikihara, A.; Nakamae, K.; Hoffman, A. S. *J. Biomater. Sci., Polym. Ed.* **2004**, *15*, 1085–1098.
- (50) Kitano, H.; Kuwayama, M.; Kanayama, N.; Ohno, K. *Langmuir* **1998**, *14*, 165–170.
- (51) Arimori, S.; Bell, M. L.; Oh, C. S.; Frimat, K. A.; James, T. D. *Chem. Commun.* **2001**, 1836–1837.
- (52) Kim, K. T.; Cornelissen, J. J. L. M.; Nolte, R. J. M.; van Hest, J. C. M. *J. Am. Chem. Soc.* **2009**, *131*, 13908–13909.
- (53) Shiomori, K.; Ivanov, A. E.; Galaev, I. Y.; Kawano, Y.; Mattiasson, B. *Macromol. Chem. Phys.* **2004**, *205*, 27–34.
- (54) Uguzdogan, E.; Kayi, H.; Denkbaz, E. B.; Patir, S.; Tuncel, A. *Polym. Int.* **2003**, *52*, 649–657.
- (55) Matsumoto, A.; Ikeda, S.; Harada, A.; Kataoka, K. *Biomacromolecules* **2003**, *4*, 1410–1416.
- (56) Ivanov, A. E.; Shiomori, K.; Kawano, Y.; Galaev, I. Y.; Mattiasson, B. *Biomacromolecules* **2006**, *7*, 1017–1024.
- (57) Pasparakis, G.; Cockayne, A.; Alexander, C. *J. Am. Chem. Soc.* **2007**, *129*, 11014–11015.
- (58) Aoki, T.; Nagao, Y.; Sanui, K.; Ogata, N.; Kikuchi, A.; Sakurai, Y.; Kataoka, K.; Okano, T. *Polym. J.* **1996**, *28*, 371–374.
- (59) Elmas, B.; Senel, S.; Tuncel, A. *React. Funct. Polym.* **2007**, *67*, 87–96.
- (60) Jin, X. J.; Zhang, X. G.; Wu, Z. M.; Teng, D. Y.; Zhang, X. J.; Wang, Y. X.; Wang, Z.; Li, C. X. *Biomacromolecules* **2009**, *10*, 1337–1345.
- (61) Shibata, H.; Heo, Y. J.; Okitsu, T.; Matsunaga, Y.; Kawanishi, T.; Takeuchi, S. *Proc. Natl. Acad. Sci. U.S.A.* **2010**, *107*, 17894–17898.
- (62) Kataoka, K.; Miyazaki, H.; Bunya, M.; Okano, T.; Sakurai, Y. *J. Am. Chem. Soc.* **1998**, *120*, 12694–12695.
- (63) Matsumoto, A.; Kurata, T.; Shiino, D.; Kataoka, K. *Macromolecules* **2004**, *37*, 1502–1510.
- (64) Zenkl, G.; Klimant, I. *Microchim. Acta* **2009**, *166*, 123–131.
- (65) Zenkl, G.; Mayr, T.; Khmant, I. *Macromol. Biosci.* **2008**, *8*, 146–152.
- (66) Lee, Y. J.; Pruzinsky, S. A.; Braun, P. V. *Langmuir* **2004**, *20*, 3096–3106.
- (67) Cambre, J. N.; Roy, D.; Gondi, S. R.; Sumerlin, B. S. *J. Am. Chem. Soc.* **2007**, *129*, 10348–10349.
- (68) Roy, D.; Cambre, J. N.; Sumerlin, B. S. *Chem. Commun.* **2008**, 2477–2479.
- (69) Roy, D.; Cambre, J. N.; Sumerlin, B. S. *Chem. Commun.* **2009**, 2106–2108.
- (70) Wang, B. L.; Ma, R. J.; Liu, G.; Liu, X. J.; Gao, Y. H.; Shen, J. Y.; An, Y. L.; Shi, L. Q. *Macromol. Rapid Commun.* **2010**, *31*, 1628–1634.
- (71) Wang, B. L.; Ma, R. J.; Liu, G.; Li, Y.; Liu, X. J.; An, Y. L.; Shi, L. Q. *Langmuir* **2009**, *25*, 12522–12528.
- (72) Kataoka, K.; Miyazaki, H.; Okano, T.; Sakurai, Y. *Macromolecules* **1994**, *27*, 1061–1062.
- (73) Jin, Q. A.; Lv, L. P.; Liu, G. Y.; Xu, J. P.; Ji, J. A. *Polymer* **2010**, *51*, 3068–3074.
- (74) Shiino, D.; Murata, Y.; Kubo, A.; Kim, Y. J.; Kataoka, K.; Koyama, Y.; Kikuchi, A.; Yokoyama, M.; Sakurai, Y.; Okano, T. *J. Controlled Release* **1995**, *37*, 269–276.
- (75) Matsumoto, A.; Yamamoto, K.; Yoshida, R.; Kataoka, K.; Aoyagi, T.; Miyahara, Y. *Chem. Commun.* **2010**, 46, 2203–2205.
- (76) Wang, L.; Liu, M. Z.; Gao, C. M.; Ma, L. W.; Cui, D. P. *React. Funct. Polym.* **2010**, *70*, 159–167.
- (77) Gan, D. J.; Lyon, L. A. *J. Am. Chem. Soc.* **2001**, *123*, 8203–8209.
- (78) Jones, C. D.; McGrath, J. G.; Lyon, L. A. *J. Phys. Chem. B* **2004**, *108*, 12652–12657.
- (79) Li, C. H.; Zhang, Y. X.; Hu, J. M.; Cheng, J. J.; Liu, S. Y. *Angew. Chem., Int. Ed.* **2010**, *49*, 5120–5124.
- (80) Hu, J. M.; Li, C. H.; Liu, S. Y. *Langmuir* **2010**, *26*, 724–729.
- (81) Kanekiyo, Y.; Sano, M.; Iguchi, R.; Shinkai, S. *J. Polym. Sci., Part A: Polym. Chem.* **2000**, *38*, 1302–1310.
- (82) Uchiyama, S.; Matsumura, Y.; de Silva, A. P.; Iwai, K. *Anal. Chem.* **2003**, *75*, 5926–5935.
- (83) Gota, C.; Okabe, K.; Funatsu, T.; Harada, Y.; Uchiyama, S. *J. Am. Chem. Soc.* **2009**, *131*, 2766–2767.
- (84) Li, C. H.; Hu, J. M.; Liu, T.; Liu, S. Y. *Macromolecules* **2011**, *44*, 429–431.